This document is the Accepted Manuscript version of a Published Work that appeared in final form in **Sensors and Actuators B: Chemical**, copyright © Elsevier Inc. after peer review and technical editing by the publisher. To access the final edited and published work see [https://doi.org/10.1016/j.snb.2018.10.021].

Colorimetric analysis of optical reflection from thin porous silicon for detection of organic liquids

I. I. Ivanov[*a,b], N. I. Klyui[*a,c], V. A. Skryshevsky[b,d]

[a]*College of Physics, Jilin University, Changchun, 2699 Qianjin St., Changchun 130012, People's Republic of China*
[b]*Institute of High Technologies, Taras Shevchenko National University of Kyiv, 64 Volodymyrska, 01033 Kyiv, Ukraine*
[c]*V. Lashkaryov Institute of Semiconductor Physics, National Academy of Sciences of Ukraine, 41 Prosp. Nauky, 03680 Kyiv, Ukraine*
[d]*Corporation Science Park Taras Shevchenko University of Kyiv, 60, Volodymyrska Str., 01033 Kyiv, Ukraine*

Abstract

A single porous silicon (PS) layer sensor structure was applied to analyze the kinetics of adsorption/desorption processes of water, ethanol and ethanol-water solution using CIE1931 chromaticity coordinates based parameters as dominant wavelength λ_{dom}, complementary wavelength λ_{com} and excitation purity (EP). Matrix method was used to obtain reflectance spectra dependences on porosity (P), PS layer thickness (L_{PS}), refractive index of analyte ($n_{analyte}$). Dependences of λ_{dom}, λ_{com}, EP on P, L_{PS}, $n_{analyte}$ were computed on the base of computed reflectance spectra and optimal parameters were determined for distinction of model analytes as water and ethanol. Time dependences of λ_{dom}, λ_{com} were experimentally obtained using CCD-based spectrometer for water, ethanol and ethanol-water solution. Advantage of characterisation of whole complex multiple peaks spectra using chromaticity parameters as opposed to sensor characterization with parameters of individual interference peaks as peak position was demonstrated.

Key words: porous silicon, CIE 1931, chromaticity coordinates, adsorption/desorption kinetic, sensor.

Introduction

Porous materials (PM) as porous silicon (PS), are a perspective and promising materials for sensor application [1]. PM characterized with large surface to volume ratio in the order of 500 -1000 m^2/cm^3 [2,3] that lets use PM for sensor application. PM properties as porosity (P), pore morphology, thickness can be controlled with etching current density and depends on wafer doping level, composition of the electrolyte [4]. The penetration of inorganic and organic molecules into pores that leads to changing of optical [5] properties of porous layer. Since the effective refractive index of a porous layer depends on refractive index of porous matrix and refractive index of the medium inside the pores. Substitution of air inside the pores after analyte infiltrated into pores causes an increase of effective refractive index of layer [6] and

shift of reflectance spectrum to longer wavelength region. Thus, by analysing the reflectance spectrum, one can detect the adsorbed molecules of analyte inside the pores.

*Corresponding authors: ivancko@gmail.com (I. I. Ivanov), klyuini@ukr.net (N. I. Klyui)

The reflectance spectrum of thin layer has form of a sequence of interference maxima and minima. Variation of peak position λ_{peak} and full width at half maximum (FWHM)) at molecule adsorption can be used as sensor parameter[7, 8]. Usually, peaks of reflectance of thin layer are wide enough that degrades the accuracy of sensor measurements. In order to monitor more precisely change of spectrum caused by analyte, the sensor structure are formed as stacks of thin PS layers such as Bragg mirror (BM), rugate filter, Fabry-Perot filter, luminescent PS microcavity [9–14]. Redshift of interference peak maxima increases with increasing of refractive index of analyte and can reaches hundreds on nm in infrared region [15]. Measurement methods as reflectometry for interference peak characterization and photoluminescence can be applied to the same sensor structure and complement one another [16]. Sensitivity of single and multiple PS layers sensor structures depends on properties of measuring optical systems and for system with spectral resolution of 0.1 nm able to detect refractive index change about 2×10^{-4} [17] and concentration of different gases and vapor in ppm range [18–20]. Noisiness of spectrums, presence of local maximums and not symmetric form of investigated peaks complicates determination of λ_{peak} and FWHM, especially for dynamically changing spectrums during adsorption/desorption processes. One can expect that the accuracy of the measurement can be increased if the spectrum as a whole is analyzed, for example, using the method CIE 1931 chromaticity color space. Now CIE 1931 chromaticity color space method is widely used for characterisation of emission spectrums of light emitted structures [21, 22]. Electromagnetic visible spectrum in range from λ_{min}=380 nm to λ_{max}=780 nm is linked with physiological perceived colors in human color vision via chromaticity coordinates as tristimulus values X, Y, Z [23, 24] in CIE 1931 chromaticity color space:

$$X = \frac{1}{N}\int_{\lambda_{min}}^{\lambda_{max}} \bar{x}(\lambda)S(\lambda)I(\lambda)\partial\lambda \tag{1a}$$

$$Y = \frac{1}{N}\int_{\lambda_{min}}^{\lambda_{max}} \bar{y}(\lambda)S(\lambda)I(\lambda)\partial\lambda \tag{1b}$$

$$Z = \frac{1}{N}\int_{\lambda_{min}}^{\lambda_{max}} \bar{z}(\lambda)S(\lambda)I(\lambda)\partial\lambda \tag{1c}$$

$$N = \int_{\lambda_{min}}^{\lambda_{max}} \bar{y}(\lambda)I(\lambda)\partial\lambda \tag{2}$$

where $S(\lambda)$ – spectral reflectance (or transmittance) of sample;

$I(\lambda)$ – spectral power distribution of a illuminant.

$\bar{x}$, $\bar{y}$, $\bar{z}$ – CIE defined color matching functions from the color matching experiments [25-27].

The color as characteristic of reflectance spectrum can be determined with the x-y parameters as coordinates (3) and can be depicted on a two-dimensional graph called the chromaticity diagram.

$$x = \frac{X}{X + Y + Z} \tag{3a}$$

$$y = \frac{Y}{X + Y + Z} \tag{3b}$$

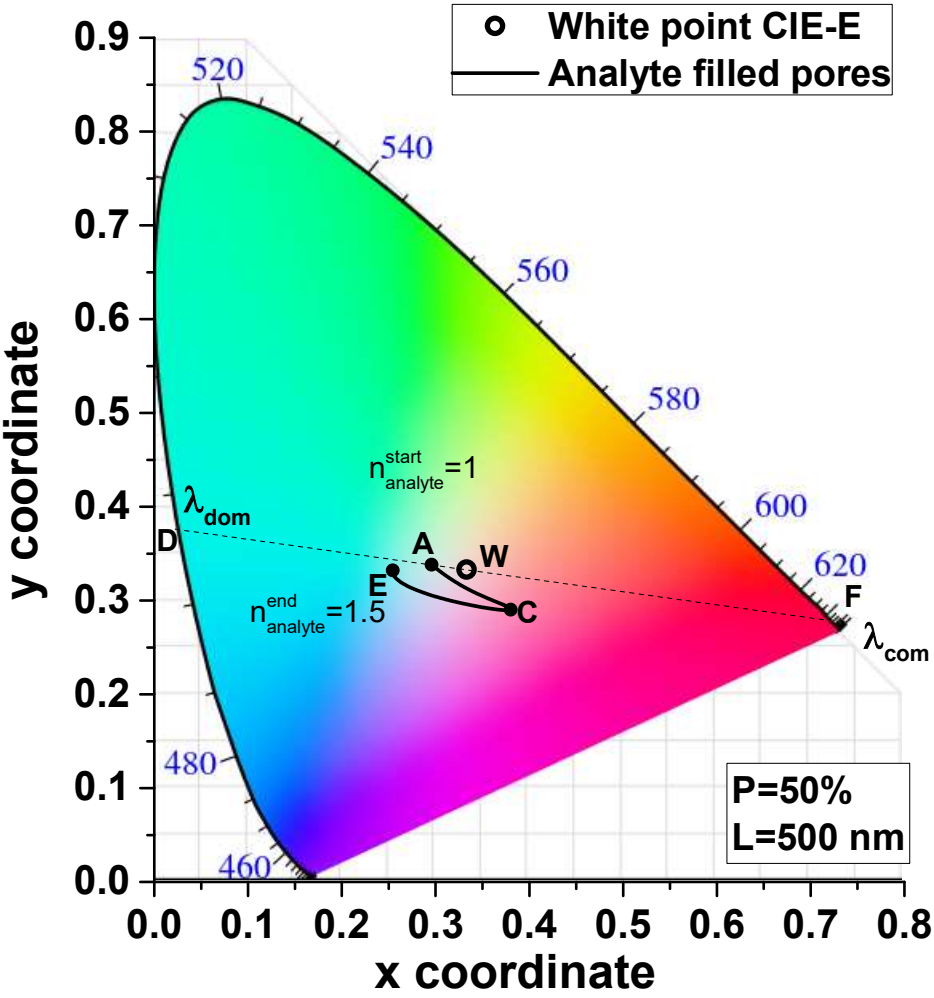

Fig. 1. CIE 1931 chromaticity diagram and computed sample color chromaticity coordinates x-y dependence on refractive index of analyte $n_{analyte}$ filling the pores (L_{PS}=500 nm, P=50%).

The outer curved boundary is the spectral locus and each point of locus represents a pure hue of a single wavelength. White illuminant in this case has coordinates x=1/3 and y=1/3 on chromaticity diagram. Point with these coordinates is called white point (point marked as ○ in Fig. 1). In the CIE color coordinate space for considered color A with x-y coordinates (Fig. 1) there is strait line between this point and the white point W. This line can be extrapolated to intersect the border of the locus. In general there can be two points of intersection (points D and F on Fig. 1). The point of intersection that is next to the considered color on extraporation curve is the dominant wavelength λ_{dom}. Considered color always lies between white point and point of intersections that determines λ_{dom}. The point of intersection on the opposite side of extrapolation line relatively to white point defines the complementary wavelength λ_{com}.

Line DF on Fig. 1 is extrapolation line. Dominant wavelength λ_{dom} and complementary wavelength λ_{com} are parameters that describe polychrome light mixtures in terms of the monochromatic light that induce an identical perception of hue in the human eye [28]. Another parameter that describes color (spectrum) in the CIE color coordinate space on chromaticity diagram is excitation purity (EP). EP is determined as ratio of segment length AW between white point W and considered color A to segment length DW between white point W and of intersection point D on extrapolation curve: EP=AW/DW. EP characterizes the saturation of a particular color. The whole spectrum with any number of spectral features can be described with only pair of parameters λ_{dom} and EP or pair λ_{com} and EP on chromaticity diagram. CIE color spaces are applied for color characterization of nanoparticle systems [29], food freshness via color change [22], PH monitoring [30], live cell characterization [31].

In present work authors analyze kinetics of adsorption and desorption by the measuring of reflectivity in single PS layer structure and express received dependences using CIE 1931 color space based parameters as λ_{dom}, λ_{com}, EP. Ethanol, water and ethanol-water solution were chosen as matter for interest. Dependences of λ_{dom}, λ_{com}, EP on L_{PS}, P were computed for wide range of refractive indexes of analyte $n_{analyte}$ inside pores.

Experimental

Samples and measurements of reflectance spectra

As subject of investigation the optical sensor based on one porous silicon layer was chosen. PS is fabricated using method of electrochemical etching of Si wafer in mixture of aqueous HF solutions and C_2H_5OH in teflon cell [1,4,7,14]. PS layers with area S=0.79 cm^2 were formed using method of electrochemical etching of p^{++}-Si wafer (0.001 Ωcm) in HF(40%):ethanol solution in teflon cell. Thermo Fisher micro pipette dispenser was used to deposit liquids analytes on the samples. After each measurement completion initial state of samples was restored using washing of samples in ethanol and drying with nitrogen flow. Control measurements of spectra after washing and drying depict the reproducibility of the initial spectra. All spectral measurements were performed with Thorlab CCD spectrometer CCS200 at 100 spectrum/s.

Position of peak maxima $\lambda^i_{peak}(n_{analyte})$ shifts to long wavelength region for pores filled with analyte $(n_{analyte})$ relatively to position of peak maxima $\lambda^i_{peak}(n_{air})$ of air (n_{air}) filled pores. All dependences of reflectance on wavelength were computed with matrix method [32-35]. Sensitivity of optical sensor is $\frac{\Delta\lambda^i_{peak}}{\Delta n}$ and depends on porosity P and PS layer thickness L_{PS}, refractive index $n_{analyte}$ (λ):

$$\frac{\Delta\lambda^i_{peak}}{\Delta n} = \frac{\lambda^i_{peak}(n_{analyte}) - \lambda^i_{peak}(n_{air})}{n_{analyte} - n_{air}} \quad (4)$$

Selectivity of optical sensor for analytes A and B can be determined as

$$\frac{\Delta\lambda^i_{peak}}{\Delta n^{A-B}_{analyte}} = \frac{\lambda^i_{peak}(n^A_{analyte}) - \lambda^i_{peak}(n^B_{analyte})}{n^A_{analyte} - n^B_{analyte}} \quad (5a)$$

or

$$\frac{\Delta R}{\Delta n_{analyte}^{A-B}} = \frac{R(n_{analyte}^{A}) - R(n_{analyte}^{B})}{n_{analyte}^{A} - n_{analyte}^{B}} \text{ at } \lambda=\text{const} \quad (5b)$$

where $\lambda_{peak}^{i}(n_{analyte}^{A})$, $\lambda_{peak}^{i}(n_{analyte}^{B})$ – position of maximum of *i*- peak of PS layer with pores filled with analytes A and B with refractive index $n_{analyte}^{A}$ and $n_{analyte}^{B}$ respectively;

$R(n_{analyte}^{A})$, $R(n_{analyte}^{A})$ – reflection coefficients of structure with pores filled with analyte A, B respectively measured at λ=const.

Accuracy of measurement of selectivity $\frac{\Delta\lambda_{peak}^{i}}{\Delta n_{analyte}^{A-B}}$ depends on accuracy of determination of maxima peaks position and depends on parameters of spectral device that used to measure reflection spectrum: spectral accuracy, spectral resolution.

Accuracy of measurement of selectivity $\frac{\Delta R}{\Delta n_{analyte}^{A-B}}$ depends on reflection coefficient R measurements at fixed λ and accordingly depends on resolution of analog to digital convertor (ADC) that transforms signal from optical transducer into electrical form. As fixed λ, at which measurements of R for set of analytes are performed, rationally to choose the position of maximum of peak $\lambda_{peak}^{i}(n_{analyte}^{A})$ for one selected basic analyte from set. Difference $R(n_{analyte}^{A}) - R(n_{analyte}^{B})$ for two analytes A and B with slightly different refractive indexes can be rather small.

Noisiness of experimental interference peaks increases with decreasing of integration time of collected signal. Noisiness and dissymmetry of peaks complicates determination of peaks positions and amplitude of peak maxima. Procedures of smoothing are used for reduction and elimination of local amplitude sharpness and mini peaks. But smoothing can lead to distortion of peak form and displacement of peaks positions that can be significant for detection of analytes with slightly different refractive index.

.

Colorimetric method

For finding λ_{dom}(or λ_{com}) and EP the reflectance spectra S(λ) of single PS layer were firstly computed using matrix method [32-35]. Tristimulus values X, Y, Z were computed on the base of S(λ) using Eq 1-2. Parameters x and y were determined from Eq. 3 to determine λ_{dom}(or λ_{com}) and EP from chromaticity diagram. Spectral dependence of refractive dependence of Si was used for computations [36]. Bruggeman effective medium model [37, 38] to link P with the refractive index of PS was used both for unfilled pores (filled with air) and pores filled with analyte.

Dependences of chromaticity coordinates x-y on refractive index of analyte were computed and depicted on chromaticity diagram (Fig. 1) for single PS layer with P=50% and L_{PS}=500 nm. Black curve ACE (Fig. 1) depicts changing of x and y parameters in accordance with changing of refractive index of analyte from $n_{analyte}^{start} = 1$ (point A) to $n_{analyte}^{end} = 1.5$ (point E) throw point C($n_{analyte}^{start} = 1.207$). As seen from

Fig. 1, there are $n_{analyte}$ ranges for which using appropriate reflectance spectra and chromaticity coordinates x-y can be calculated and both λ_{dom} and λ_{com} can be determined. Both λ_{dom} and λ_{com} varies in wide range of wavelengths and variation depends on initial porosity of layer and L_{PS}.

To estimate the magnitude of the change of λ_{dom}, λ_{com}, EP in comparison with change of interference peak #1 (peak #1 is the first long wavelength interference peak in considered wavelength region determined from reflectance spectra) position caused by filling pores analyte with refractive index $n_{analyte}$ in range 1.31..1.41 corresponding computed dependences are depicted in Fig. 2 for structure with P=70% and L_{PS}=500 nm. Shift of position of peak #1 maximum of methanol filled pores comparatively to propanol filled pores is $\Delta\lambda_{peak1}^{shift}$ (propanol-methanol)=$\lambda_{peak1}(n_{propanol})$-$\lambda_{peak1}(n_{methanol})$=14 nm and $\Delta\lambda_{peak1}^{shift}/\Delta n$=276.1. For analyte pair as water and ethanol computed parameters are $\Delta\lambda_{peak1}^{shift}$=7 nm and $\Delta\lambda_{peak1}^{shift}/\Delta n$=244. Shift of chromaticity parameters λ_{dom}, λ_{com} and EP as characteristic of whole spectra are

$$\Delta\lambda_{dom}^{shift}(analyte\ A - analyte\ B) = \lambda_{dom}^{shift}\left(n_{analyte\ B}\right) - \lambda_{dom}^{shift}\left(n_{analyte\ A}\right) \quad (6a)$$

$$\Delta\lambda_{com}^{shift}(analyte\ A - analyte\ B) = \lambda_{com}^{shift}\left(n_{analyte\ B}\right) - \lambda_{com}^{shift}\left(n_{analyte\ A}\right) \quad (6b)$$

$$\Delta EP_{shift}(analyte\ A - analyte\ B) = EP_{shift}\left(n_{analyte\ B}\right) - EP_{shift}\left(n_{analyte\ A}\right) \quad (6c)$$

where

$$\lambda_{dom}^{shift}\left(n_{analyte}\right) = \lambda_{dom}\left(n_{analyte}\right) - \lambda_{dom}\left(n_{air}\right) \quad (7a)$$

$$\lambda_{com}^{shift}\left(n_{analyte}\right) = \lambda_{com}\left(n_{analyte}\right) - \lambda_{com}\left(n_{air}\right) \quad (7b)$$

$$EP_{shift} = EP\left(n_{analyte}\right) - EP\left(n_{air}\right) \quad (7c)$$

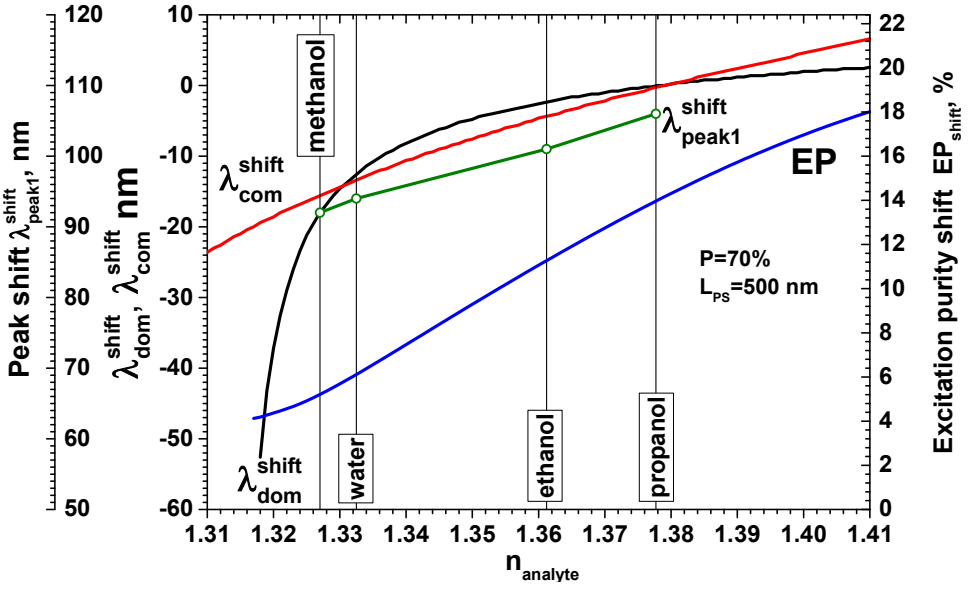

Fig. 2. Computed dependence of shift of dominant λ_{dom}^{shift}, complementary wavelength λ_{com}^{shift}, the excitation purity EP_{shift}, position of diffraction peak λ_{peak1}^{shift} on refractive index of analyte $n_{analyte}$ inside the pores. Vertical lines depict the value of refractive index for methanol, water, ethanol, propanol.

Table 1

Shift of chromaticity parameters λ_{dom}, λ_{com} and EP for different pairs of analytes

Parameter	Pair of analytes			
	Analyte A	Analyte B	Analyte A	Analyte B
	methanol	propanol	water	ethanol
$\Delta\lambda_{peak1}^{shift}$, nm	13		7.6	
$\Delta\lambda_{peak2}^{shift}$, nm	10.2		5.2	
$\Delta\lambda_{peak3}^{shift}$, nm	6.8		3.7	
$\Delta\lambda_{dom}^{shift}$, nm	17.9		10.5	
$\Delta\lambda_{com}^{shift}$, nm	15.7		8.9	
EP_{shift}, nm	8.8		5.16	
$\Delta\lambda_{dom}^{shift} / \Delta n$	351		362	
$\Delta\lambda_{com}^{shift} / \Delta n$	307.8		306	
$EP_{shift} / \Delta n$	172.5		178	

Determined values from Fig. 2 are depicted in Table 1. Comparison of shift of tree interference peaks $\Delta\lambda_{peak1,2,3}^{shift}$ determined from reflectance spectra calculated by matrix method [32-35] with shift of $\Delta\lambda_{dom}^{shift}$, $\Delta\lambda_{com}^{shift}$ and EP_{shift} shows that parameters λ_{dom}, λ_{com}, EP can be used for reflectance spectrum characterisation and characterisation of changing of spectrum caused different analyte filling of pores. Magnitude of parameters $\Delta\lambda_{dom}^{shift}$, $\Delta\lambda_{com}^{shift}$ and EP_{shift} that proposed for reflectance spectra characterization is larger then magnitude of interference peak shift $\Delta\lambda_{peak1}^{shift}$ that traditionally used for characterization of spectrum with interference maxima and minima.

Numerical analysis

Dependences of λ_{dom}, λ_{com} and EP on porosity P and refractive index of analyte that fill pores were computed. Computed in accordance with Eq. 7 shift of $\lambda_{dom}(n_{analyte})$, $\lambda_{com}(n_{analyte})$, $EP(n_{analyte})$ for analyte filled pores relatively to values $\lambda_{dom}(n_{air})$, $\lambda_{com}(n_{air})$, $EP(n_{air})$ for unfilled analyte pores (L_{PS}=500nm) are depicted in Fig. 3, respectively. There are some ranges of P (for fixed L_{PS}) and $n_{analyte}$ where λ_{dom} can not be defined due to definition of λ_{dom}. These areas are marked with square filling. For PS layers with low porosity P<30% λ_{dom} practically isn't depend on $n_{analyte}$. Value of $|\Delta\lambda_{dom}^{shift}|$ increases with P increasing and can reach 170 nm for certain $n_{analyte}$.

There is limit of maximum value of porosity that can be experimentally fabricated due to mechanical strength of PS layers of high porosity caused by internal mechanical tension of porous layer through oxidation in air [39]. From practical point of view it is more important to consider difference of λ_{dom} or $\Delta\lambda_{dom}^{shift}$ for defined set of analytes with defined range $n_{analyte}^{min}...n_{analyte}^{max}$, where $n_{analyte}^{min} > n_{air}$=1. Vertical

lines on Fig. 3 show refractive index range $n_{water} = n_{analyte}^{min} ... n_{analyte}^{max} = n_{ethanol}$ that is analyzed later. Values of $|\lambda_{dom}^{shift}|$, $|\lambda_{com}^{shift}|$, $|EP_{shift}|$ increases for higher values of P.

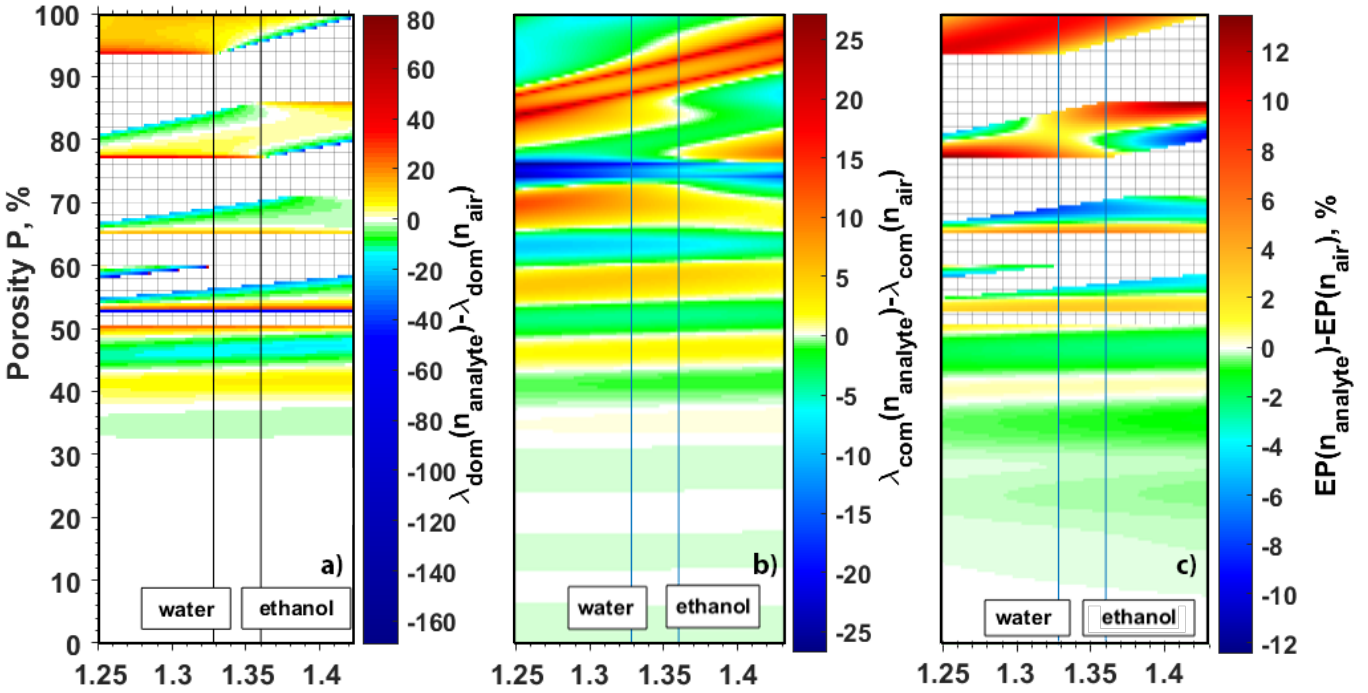

Fig. 3. Computed dependence of shift of dominant wavelength $\lambda_{dom}(n_{analyte})$ (a), complementary wavelength $\lambda_{com}(n_{analyte})$ (b), $EP(n_{analyte})$ (c) on layer porosity and refractive index of analyte $n_{analyte}$ inside the pores relatively to $\lambda_{dom}(n_{air})$, $\lambda_{com}(n_{air})$, $EP(n_{air})$ of air filled pores, respectively.

Dependence of λ_{dom}, λ_{com}, EP on P, $n_{analyte}$ gives 2D matrix as result of computation (Fig. 3). Values λ_{dom}, λ_{com}, EP also depend on L_{PS}. Dependences of difference $\Delta\lambda_{dom}(ethanol - water) = \lambda_{dom}(n_{ethanol}) - \lambda_{dom}(n_{water})$, $\Delta\lambda_{com}(ethanol - water) = \lambda_{com}(n_{ethanol}) - \lambda_{com}(n_{water})$ on P for water (n_{water}= 1.3236) and ethanol ($n_{ethanol}$= 1.3558) were considered to simplify further analysis and data visualisation. Factually computed dependences are dependences of differences of profiles at fixed n_{water} and $n_{ethanol}$ specified as line on 3D plot in Fig. 3.

From practical point of view, for sensor application to receive higher sensitivity $\Delta\lambda_{dom}/\Delta n$, $\Delta\lambda_{com}/\Delta n$, for selected range Δn the optimal parameters P and L_{PS} that determines maxima $|\Delta\lambda_{dom}|$, $|\Delta\lambda_{com}|$, should be found (Fig. 4).

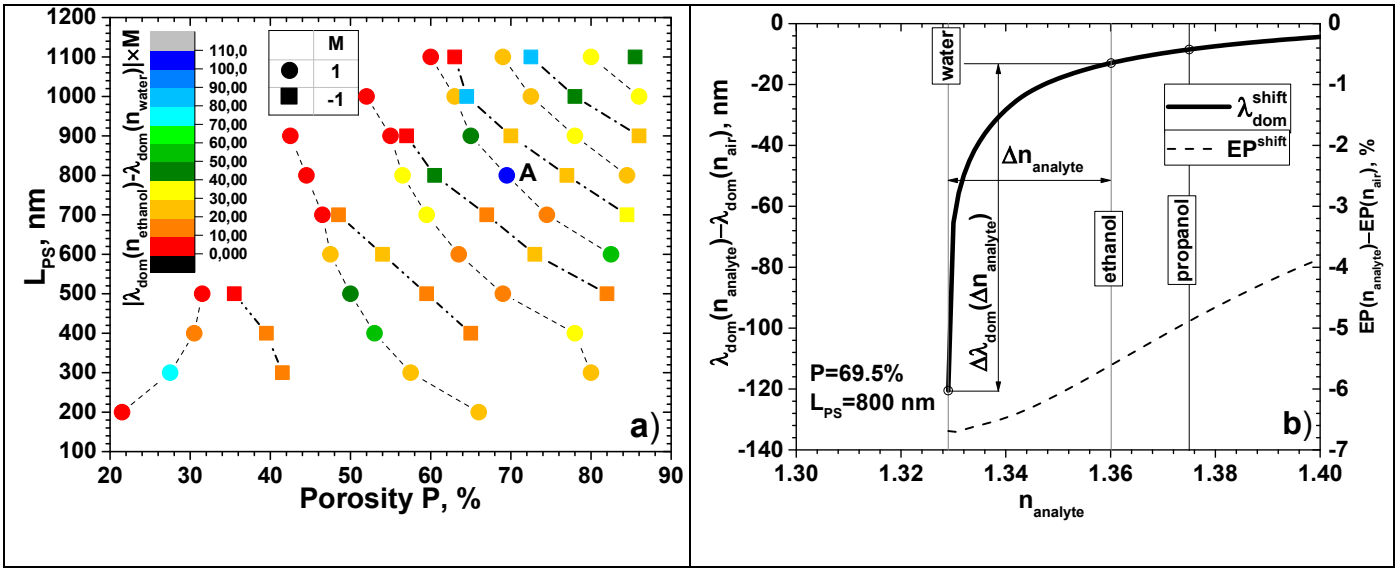

Fig. 4. a) Computed dependence of local maximums of difference $|\lambda_{dom}(n_{ethanol})-\lambda_{dom}(n_{water})|$ on porosity P and PS layer thickness L_{PS}; b) computed dependence of shift of dominant wavelength $\lambda_{dom}(n_{analye})$ and excitation purity $EP(n_{analyte})$ for analyte filled pores in reference to $\lambda_{dom}(n_{air})$ and $EP(n_{air})$ of air filled pores respectively on refractive index of analyte $n_{analyte}$ inside the pores for PS thickness L_{PS}=800 nm and P=69.5% (point A, Fig. 4a).

Local maxima represented on Fig. 4a with circles, local minima with squares. For sample with certain L_{PS} there can be several local maxima and minima at discrete values of P. Analysis of dependence of $|\Delta\lambda_{dom}|$ on discrete values P and L_{PS} shows that position of local maxima $|\Delta\lambda_{dom}|$ is described with uninterrupted curves on plane of P and L_{PS} variables. These continuous curves that depicts dependence of maxima of $|\lambda_{dom}(n_{ethanol})-\lambda_{dom}(n_{water})|$ on L_{PS} and P are displayed as dotted lines in Fig. 4a. So, to receive maximum response of sensor as maximum values of $|\lambda_{dom}(n_{ethanol})-\lambda_{dom}(n_{water})|$ for analyte as ethanol and water one should choose point on these curves for desired L_{PS} and P. Analyze of $|\lambda_{dom}(n_{ethanol})-\lambda_{dom}(n_{water})|$ values along dotted lines on Fig. 4a shows presence of maximums: 52.5 nm (L_{PS}=400 nm, P=53%), 37 nm (L_{PS}=800 nm, P=56.5%), 102.7 nm (L_{PS}=800 nm, P=69.5%), 32 nm (L_{PS}=900 nm, P=78%)…

Computed dependence of maximum shift of dominant wavelength $\lambda_{dom}(n_{analye})$ and excitation purity $EP(n_{analyte})$ in reference to $\lambda_{dom}(n_{air})$ and $EP(n_{air})$ respectively on refractive index of analyte $n_{analyte}$ for structure with L_{PS}=800 nm and P=69.5% (point A, Fig. 4a) is shown on Fig. 4b. For pair water and ethanol $|\lambda_{dom}(n_{ethanol})-\lambda_{dom}(n_{water})|$ is 102.7 nm and $EP(n_{ethanol})-EP(n_{water})$=1.21%. For pair propanol and ethanol $|\lambda_{dom}(n_{propanol})-\lambda_{dom}(n_{ethanol})|$ is 4.8 nm and $EP(n_{propanol})-EP(n_{ethanol})$ is 0.73%. These values for ethanol-propanol are less comparatively with values for ethanol-water because parameters L_{PS} and P are optimal for analyte pair as ethanol-water. Optimal parameters P for any pair of analyte as

analyte A−analyte B can be determined from Fig. 3 for structure with L_{PS}=500 nm. To receive optimal parameters L_{PS} dependences as depicted on Fig. 3 should be computed for different values of L_{PS}.

Adsorption/desorption kinetics

Experimental dependence of reflection coefficient on time for PS sample (L_{PS}=600 nm, P=50%) with pores filled with ethanol depicted in Fig. 5. Initial time t_0 is moment of beginning of deposition of ethanol on the surface of PS sample. There are transition processes related with analyte deposition and pores filling during time interval $t_0..t_1$. Time range $t_1 < t < t_2$ corresponds to the state when pores are filled with analyte and analyte is evaporated from surface. Positions of peaks maximums practically doesn't change during analyte evaporation from sample surface due pores are still filled with analyte. Thickness of liquid analyte layer on the surface of sample decreases with time due to analyte evaporation and this results in jitter of widths of interference peaks maximums in time range $t_1 < t < t_2$. The invariance of the position of the interference peaks and the jitter of the peak width upon evaporation of the analyte from the PS surface was shown as a result of computer simulation in work [35, 40]. Desorption of analyte molecules from pores begins at t_2 and is described by time range $t_2..t_3$. Region $t>t_3$ accords to state when PS layer reflectance spectrum came back to initial state, i.e. to full analyte desorption both from PS surface and pores. Reflectance spectrum has non monotonic behavior during desorption in region $t_2..t_3$. Reflectance spectrum shape change at $t>t_3$ comparatively to initial spectrum at $t<t_0$ can be caused by presence of un-desorbed molecules of analyte inside pores and depends on interactions of analyte molecules with molecules that form pores.

Filling of pores with liquid analyte or in other words replacement of air inside the pores with an analyte results to clear shift of interference peaks due to large difference of refractive index of air and liquids. But difference of interference peaks position can be small for analytes that have small refractive index difference. Detectable interference peaks position difference depends on spectrometer parameters, noise level, parameters of porous structure.

Reflectance spectrums for PS structure (L_{PS}=500 nm, P=50%) with pores completely filled with water and ethanol after completion of all transient processes are shown in Fig. 6. Integration time of measured separate spectrums was 50 ms to measure kinetics of adsorption/desorption processes. Experimental spectrums are noised and were smoothed to determine positions of peaks maximums. Shifts of positions of peaks maximums in observed wavelength range are λ^1_{shift}=9 nm (long wavelength peak), λ^2_{shift}=2.8 nm, λ^3_{shift}=1.5 nm (short wavelength peak). Peak shift λ_{shift} is larger for peaks in long wavelength part of spectrum but simultaneous widening of peaks and noisiness complicates peak position determination. At moment t_2 desorption processes from pores starts. These processes accompanied by the reallocation of analyte inside pores and on the surface of sample that result to complicate form of reflectance spectrum, splitting of peaks (Fig. 6 inset). Presence of complex shape peaks with several local maxima makes impossible to determine the exact position of the peaks especially if analytes with slightly different refractive indexes are considered.

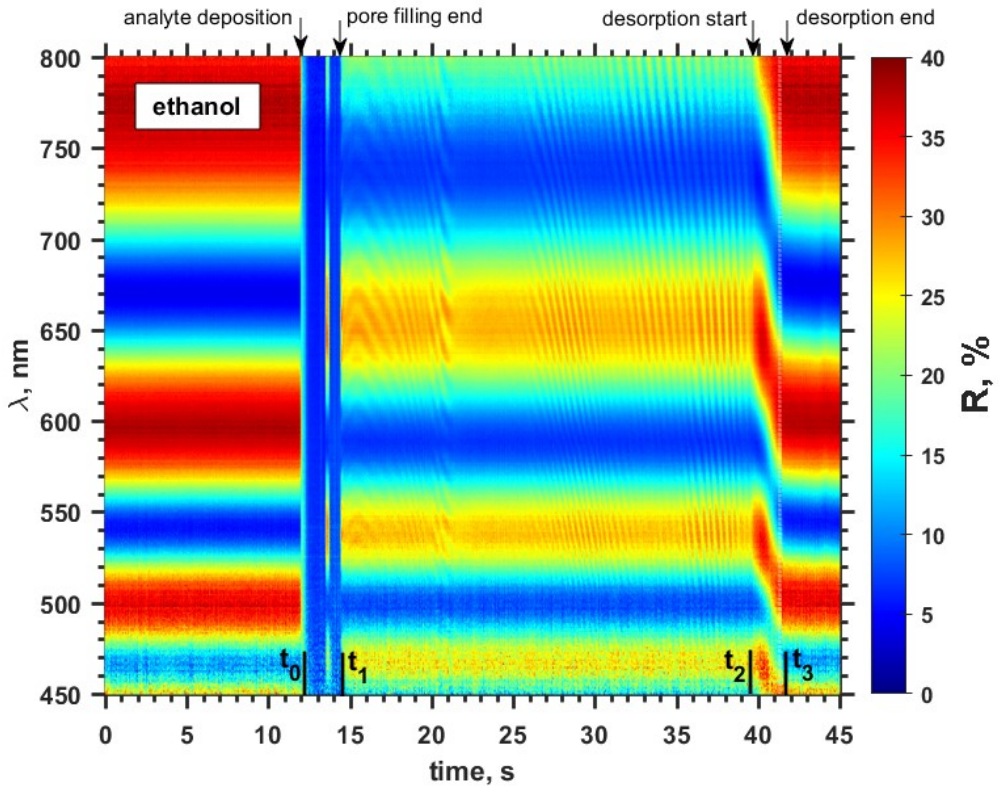

Fig. 5. Experimental dependence of reflection coefficient on time for sample with one PS layer (L_{PS}=600 nm, P=50%) filled with ethanol.

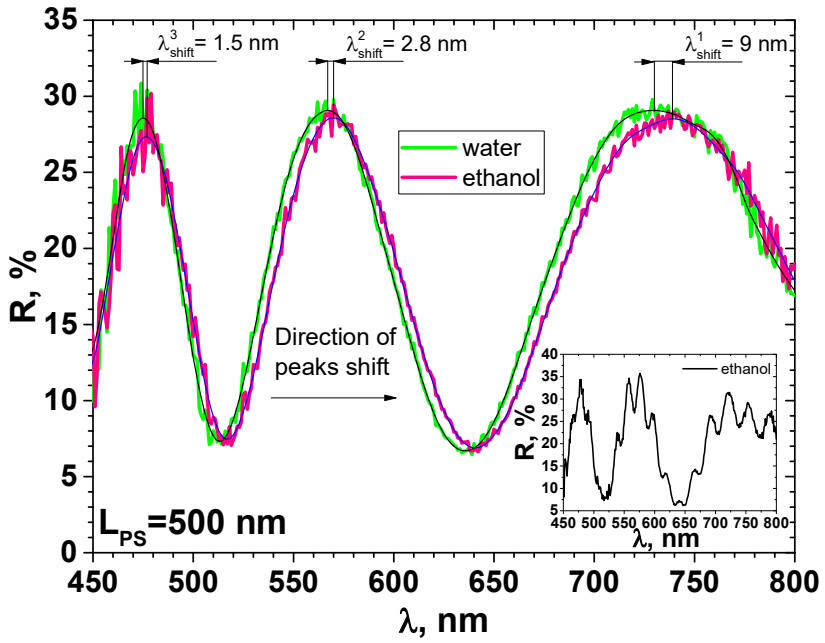

Fig. 6. Experimental dependence of reflection coefficient on wavelength for sample with PS layer (L_{PS}=500 nm, P=50%) filled with water and ethanol in stationary state and transient state (inset).

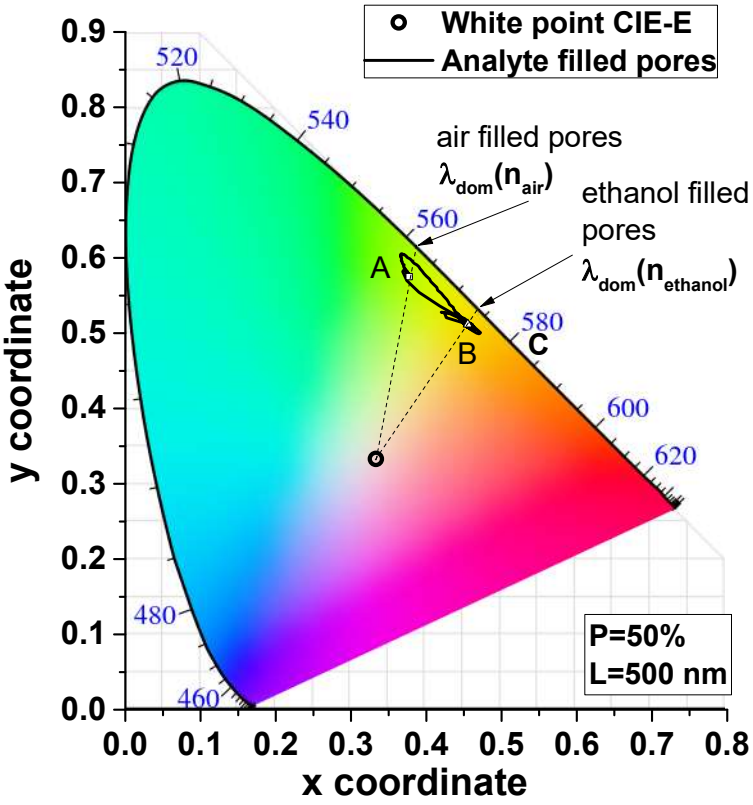

Fig.7. 1931 chromaticity diagram and shift of experimental sample color chromaticity coordinates x-y after pores filling with ethanol (L_{PS}=500 nm, P=50%).

Chromaticity coordinates x-y were computed on the base of dependence of reflectance spectra (λ_{min}=420 nm to λ_{max}=780 nm) on time for PS sample (L_{PS}=500 nm, P=50%) with pores filled with ethanol as analyte (Fig. 7). Wavelength λ_{min}=420 nm was chosen as lower limit for measurement to avoid spectra noiselessness at λ<420 nm during analysis of kinetics of adsorption/desorption processes. Increased noise is observed in short wavelength range due to decreasing of the grating efficiency of used CCD spectrometer and small integration time required for measurement of the quickly changing spectrum. Point A represents reflectance spectrum for pores filled with air. Point B represents reflectance spectrum for pores filled with ethanol. For unfilled pores $\lambda_{dom}(n_{air})$=563 nm and for pores filled with ethanol $\lambda_{dom}(n_{ethanol})$=574 nm. All chromaticity coordinates and chromaticity parameters λ_{dom}, λ_{com}, EP were computed for measured reflectance spectrums limited with range λ_{min}=450 nm to λ_{max}=780 nm to avoid the influence of noisy low wavelength range peaks.

Kinetic of adsorption/desorption processes for ethanol and water expressed as dependence of $\lambda_{dom}^{shift}(n_{analyte}) = \lambda_{dom}(n_{analyte}) - \lambda_{dom}(n_{air})$ and $\lambda_{com}(n_{analyte})$ on time is depicted on Fig. 8a for PS sample with L_{PS}=500 nm and P=50%. Dependences for ethanol and water were aligned relative to the time t_0 of analyte deposition. There are transition processes related with analyte deposition and pores filling in the range $t_0..t_1$. Clear shift of λ_{dom} and λ_{com} is observed after completion of transition processes and complete filling of pores with analyte at moment t_1. Shift $\lambda_{dom}^{shift}(n_{ethanol})$ of $\lambda_{dom}(n_{ethanol})$ for sample with pores filled with ethanol relatively of $\lambda_{dom}(n_{air})$ for unfilled pores is 10.3 nm. For pores filled with water

$\lambda_{dom}^{shift}(n_{water}) = \lambda_{dom}(n_{water}) - \lambda_{dom}(n_{air})$ =8.7 nm. Difference of λ_{dom}^{shift} for ethanol and water is $\Delta\lambda_{dom}(\text{ethanol} - \text{water}) = \lambda_{dom}^{shift}(n_{ethanol}) - \lambda_{dom}^{shift}(n_{water}) =$ 1.6 nm and ratios are $\Delta\lambda_{dom}$(ethanol-water)/($n_{ethanol}$−n_{water})=43 and $\Delta\lambda_{com}$(ethanol-water)/($n_{ethanol}$−n_{water})=446.2. Dependences of $\Delta\lambda_{dom}=\lambda_{dom}(C_2H_5OH\text{-}H_2O$ mixture)$-\lambda_{dom}(H_2O)$ and $\Delta\lambda_{com}=\lambda_{com}(C_2H_5OH\text{-}H_2O$ mixture)$-\lambda_{com}(H_2O)$ on ethanol/water volume ratio can help to distinguish mixtures of water and ethanol (Fig. 8b).

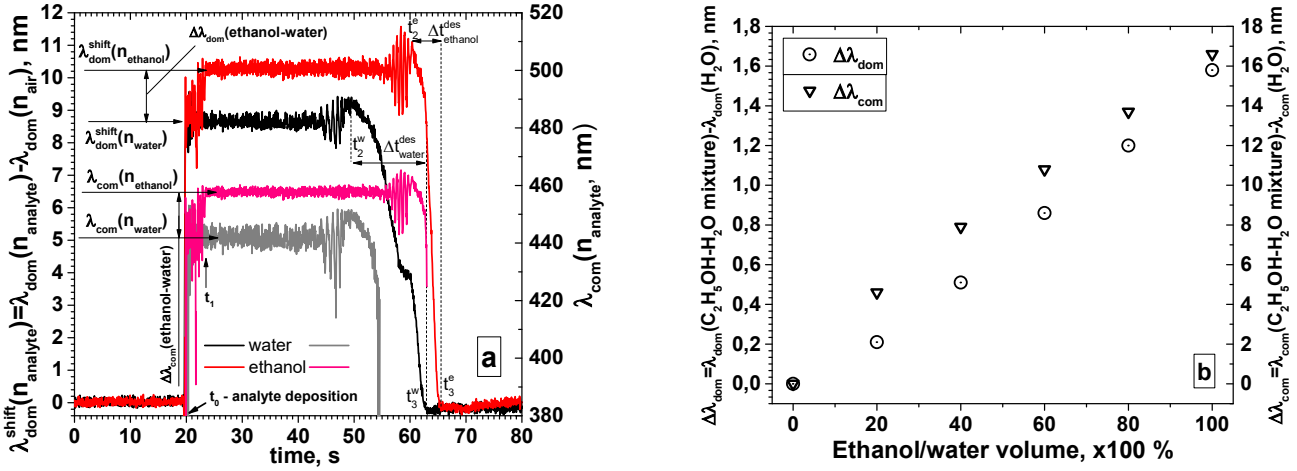

Fig. 8. a) experimental dependence of shift of dominant wavelengths $\lambda_{dom}^{shift}(n_{ethanol})$, $\lambda_{dom}^{shift}(n_{water})$ and dependence of complementary wavelengths $\lambda_{com}(n_{ethanol})$, $\lambda_{com}(n_{water})$ on time after deposition of ethanol and water on sample surface and pores filling (L_{PS}=500 nm, P=50%); b) experimental dependence of $\Delta\lambda_{dom}$, $\Delta\lambda_{com}$ on ethanol/water volume ratio (L_{PS}=500 nm, P=50%).

As was shown before whole spectrum can be characterized with λ_{dom} or λ_{com}. Value of $\Delta\lambda_{com}$ shifts up to 442 nm after filling of pores with water and shifts up to 457 nm after filling of pores with ethanol. Difference of λ_{com} for pores filled with ethanol and water is $\Delta\lambda_{com}(\text{ethanol} - \text{water}) = \lambda_{com}(n_{ethanol}) - \lambda_{com}(n_{water}) = 15$ nm. Value λ_{com} isn't defined for time $t<t_0$ and for times after desorption of analytes from pores starts due definition of λ_{com}. Ratio $\Delta\lambda_{com}$(ethanol-water)/($n_{ethanol}$−n_{water})=403. Desorption of analytes begins at t_2^e and t_2^w and ends at t_3^e and t_3^w for ethanol and water respectively. Different time of analyte desorption from pores $\Delta t_{ethanol}^{des} < \Delta t_{waterl}^{des}$ is explained with the difference in wettability and interaction of water and alcohol molecules with silicon walls in the pores

Kinetic of adsorption/desorption processes for ethanol, water and solution ethanol-water (1:1) was investigated and depicted as dependence of $\lambda_{dom}^{shift}(n_{analyte}) = \lambda_{dom}(n_{analyte}) - \lambda_{dom}(n_{air})$ on time on Fig. 9 for PS sample with L_{PS}=600 nm and P=50%. Dependences for all analytes were aligned relative to the time t_0 of analyte deposition start. After completion of transients processes at t_1 value λ_{dom}^{shift} stays practically constant till beginning of desorption processes at t_2. For investigated analytes there is

relation $\lambda_{dom}^{shift}(n_{water}) < \lambda_{dom}^{shift}(n_{ethanol-water\,1:1}) < \lambda_{dom}^{shift}(n_{ethanol})$. This relationship is confirmed by computer simulation on Fig. 4b were $\lambda_{dom}^{shift}(n_{water}) < \lambda_{dom}^{shift}(n_{ethanol})$.

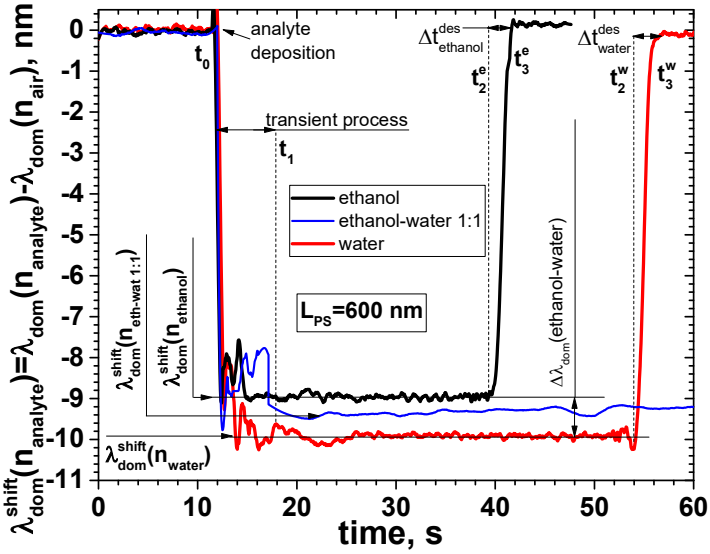

Fig. 9. Experimental dependence of shift of dominant wavelengths $\lambda_{dom}^{shift}(n_{ethanol})$, $\lambda_{dom}^{shift}(n_{water})$, $\lambda_{dom}^{shift}(n_{ethanol-water})$ on time after deposition of ethanol, water and ethanol-water solution (1:1) on sample surface and pores filling (L_{PS}=600 nm, P=50%).

Conclusion

CIE 1931 color space based parameters as λ_{dom}, λ_{com}, EP can describe kinetics of adsorption/desorption processes of analyte in PS single layer structure. Colorimetric analysis based on parameters as λ_{dom} or λ_{com} characterizes spectrum changing as whole contrary to determination of changing of parameters of separate spectrum features as interference peaks. Computed dependences of λ_{dom}, λ_{com}, EP on porosity (P), PS layer thickness (L_{PS}) shown the presence of sets [P, L_{PS}] where maximum selectivity is observed for analytes with refractive indexes in the range $n_{min}…n_{max}$. Time dependences of λ_{dom}, λ_{com} show complex behaviour at adsorption/desorption of ethanol, water and ethanol-water solution. Ratios $\Delta\lambda_{dom}$(ethanol-water)/($n_{ethanol}-n_{water}$)=43 and $\Delta\lambda_{com}$(ethanol-water)/($n_{ethanol}-n_{water}$)=403 were experimentally obtained for ethanol and water. Using parameters as λ_{dom}, λ_{com}, EP is attractive approach to reduce data matrix dimension or number of sensor elements in sensor matrix of electronic tongue/nose based on single PS layer.

Acknowledgements

This work was partially supported by the national long-term project No WQ20142200205 of “Thousand Talents Plan of Bureau of Foreign Experts Affairs” of the People’s Republic of China, Programme H2020-MSCA-RISE-2015 (Project 690945 “Carther”) and STCU Project 6362 “Promising functional nanomaterials on the base of silicon and carbon for modern sensors and optoelectronics”

Literature

1. M.J. Sailor, Porous Silicon in Practice: Preparation, Characterisation and Application, Wiley-VCH, Singapore, 2012.
2. M. du Plessis, Relationship between specific surface area and pore dimension of high porosity nanoporous silicon - Model and experiment, Phys. Status solidi A. 204(2007) 2319-2328.
3. A. Bragaru, M. Simion, K. Mihaela, T. Ignat, I. Kleps, V. Schiopu-Tucureanu, A.M. Avram and F. Craciunoiu, Study of the nanostructurated silicon chemical functionalization, Rom. J. Inf. Sci. Tech. 11(2008) 397-407.
4. D. Losic, A. Santos, Electrochemically engineered nanoporous materials, Springer, Switzerland, 2015.
5. G. Marsh, Porous silicon a useful imperfection, Mater. Today 5(2002) 36-41.
6. N. Koshida, Device applications of silicon nanocrystals and nanostructures, Springer Science & Business Media, New York, 2008.
7. G. Korotcenkov, Porous silicon: from formation to application. Formation and properties, CRC Press, Boca Raton, 2016.
8. H. Zhang, Z. Jia, X. Lv , J. Zhou , L. Chen, R. Liu and J. Ma, Porous silicon optical microcavity biosensor on silicon-on-insulator wafer for sensitive DNA detection, Biosens. Bioelectron 44(213) 89-94.
9. O. Bisi, S. Ossicini, L. Pavesi, Porous silicon: a quantum sponge structure for silicon based optoelectronics, Surface Science Reports 38(2000) 1–126.
10. S. Chan, P.M. Fauchet, Y. Li, L.J. Rothberg, B.L. Miller, Porous silicon microcavities for biosensing applications, Physical. Status. Solidi A 182(2000) 541–546.
11. P. Bettotti, M. Cazzanelli, L. Dal Negro, B. Danese, Z. Gaburro, C.J. Oton, et al., Silicon nanostructures for photonics, Journal of Physics: Condensed Matter 14(2002) 8253–8281.
12. H. Ouyang, P.M. Fauchet, Biosensing using porous silicon photonic bandgap structures, Proceedings of the SPIE 6005(2005) 31–45.
13. P. A. Snow, E.K. Squire, P. St, J. Russek, L.T. Canham, Vapor sensing using the optical properties of porous silicon Bragg mirrors, Journal of Applied Physics 86 (1999) 1781–1784.
14. G. Korotcenkov, B.K. Cho, Porous semiconductors: advanced material for gas sensor applications, CRC Cr. Rev. Sol. State. 35 (2010) 1–37.
15. L. De Stefano, L. Moretti, I. Rendina and A. M. Rossi, Porous silicon microcavities for optical hydrocarbons detection, Sensors and Actuators A 104(2003) 179-182.
16. Z. Gaburro, N. Daldosso, L. Pavesi, G. Faglia, C. Baratto, and G. Sberveglieri, Monitoring penetration of ethanol in a porous silicon microcavity by photoluminescence interferometry, Applied Physics Letters, 78(2001) 3744- 3746.
17. D. L. Andrews, Z. Gaburro, Frontiers in surface nanophotonics: principles and applications, Springer, New York, 2007.

18. M. Rocchia, E. Garrone, F. Geobaldo, L. Boarino, M.J. Sailor, Sensing CO2 in a chemically modified porous silicon film, Physical Status Solidi A 197 (2003) 365–369.
19. S. Letant, M.J. Sailor, Detection of HF gas with porous silicon interferometer, Advanced Materials 12 (2000) 355–359.
20. L. De Stefano, L. Moretti, I. Rendina, A.M. Rossi, Porous silicon microcavities for optical hydrocarbons detection, Sensors and Actuators A 104 (2003) 179–182.
21. R. K. Tamrakar, D.P. Bisen, K. Upadhyay, M. Sahu, I. P. Sahu, and N. Bramhe, Comparison of emitted color by pure Gd2O3 prepared by two different methods by CIE coordinates, Superlattice. Microst 88(2015) 382-388.
22. C. Schaude, C. Meindl, E. Fröhlich, J. Attard, G. J.Mohr, Developing a sensor layer for the optical detection of amines during food spoilage, Talanta 170 (2017) 481-487.
23. R.W. Hunt, M. R. Pointer, Measuring Colour, Wiley, 2011.
24. R.F. Wolffenbuttel, G. DeGraaf, Performance of an integrated silicon colour sensor with a digital output in terms of response to colours in the colour triangle, Sensor. Actuat A-Phys. 22(1990) 574-580.
25. W. D. Wright, The Measurement of Colour, Hilger Limited, London 1969.
26. Colour & Vision Research laboratory and database, http://cvrl.ioo.ucl.ac.uk
27. Colour Measurement: Principles, Advances and Industrial Applications, Woodhead Publishing Limited, Oxford, 2010.
28. J. P. Dakin, R. Brown, Handbook of optoelectronics: concepts, devices, and techniques, CRC press, 2017.
29. A. Chhatre, P. Solasa, S. Sakle, R. Thaokar, A. Mehra, Colloid. Surface. A 404(212) 83-92.
30. J. Pramila, D. S. Kim, An ultrasensitive method of real time pH monitoring with complementary metal oxide semiconductor image sensor, Anal. Chim. Acta. 858(2015), 55-59.
31. B. Shi, Y. Gao, C. Liu, W. Feng, Z. Lia, L. Wei, M. Yu, ratiometric fluorescent sensor for pH fluctuation and its application in living cells with low dark toxicity, Dyes and Pigments 136(2017) 522-528.
32. A. Thelen, Design of Optical Interference Coatings, McGraw-Hill, New York, 1989.
33. J.A. Dobrowolski, Optical properties of films and coatings, in: M. Bass (Ed.), Handbook of Optics, vol. 1, McGraw-Hill, New York, 1995.
34. P. Yeh, Optical Waves in Layered Media, Wiley, New York, 1988.
35. I.I. Ivanov, V.A. Skryshevsky, T. Serdiuk, V. Lysenko, Kinetics of adsorption–desorption processes of alcohol molecules in porous silicon Bragg mirror, Sensor Actuat. B. 174(2012) 521-526.
36. Refractive index database, www.refractiveindex.info.
37. M. Khardani, M. Bouaïcha, B. Bessaïs, Bruggeman effective medium approach for modelling optical properties of porous silicon: comparison with experiment, Phys. Status Solidi C 4 (2007) 1986–1990.

38. D Stroud, The effective medium approximations: Some recent developments, Superlattices Microst. 23(1998) 567-573.
39. E.V. Astrova, V.A. Tolmachevb, Effective refractive index and composition of oxidized porous silicon films, Mat. Sci. Eng. 69(2000), 142-148.
40. Nickolai I. Klyui, Ivan I. Ivanov, Oleksandr S. Kyslovets, Lyubov V. Avksentyeva, Valeriy A.Skryshevsky. Features of the use of optical reflection from thin porous silicon for detection of organic liquid, Sensor Actuat B, 242 (2017) 1177-1185.